Journal of *Marine Science and Engineering*

MDPI

Article

Modelling of Synthetic Fibre Rope Mooring for Floating Offshore Wind Turbines

Stian H. Sørum [1], Nuno Fonseca [1,*], Michael Kent [2] and Rui Pedro Faria [2]

[1] SINTEF Ocean, NO-7093 Trondheim, Norway
[2] Bridon-Bekaert, Coatbridge ML5 2AG, UK
* Correspondence: nuno.fonseca@sintef.no

Abstract: Fibre ropes offer beneficial properties for mooring of floating offshore wind turbines (FOWTs). However, the mooring line's stiffness is both load-history and load-rate dependent. A quasi-static stiffness is observed for slow loading, with a higher stiffness related to rapid, cyclic loading (dynamic stiffness). Design standards provide different guidelines for how to combine these in the mooring analysis. This paper describes procedures for adapting laboratory test stiffness results to the Syrope and a bi-linear model and investigates the consequence of using the models for load calculations. The Syrope model accounts for the quasi-static and permanent rope elongation, while performing the analyses with the dynamic stiffness. The bi-linear model applies both the quasi-static and dynamic stiffness in the dynamic analyses. Based on fibre rope tests performed by Bridon-Bekaert, a Syrope model and two bi-linear models are adapted to the same fibre rope. Fatigue damage and ultimate loads on the mooring lines of Saitec's SATH FOWT are calculated. The bi-linear model artificially reduces the tension ranges, particularly if there is a large difference between the quasi-static and dynamic stiffness of the fibre rope. This leads to a longer predicted fatigue lifetime. Differences in the extreme loads are caused by the permanent elongation of the Syrope model. This may be countered if the elongation is known and included in the bi-linear model. Finally, the bi-linear model introduces an amplitude-dependency in the horizontal natural periods.

Keywords: floating offshore wind turbines; synthetic mooring lines; quasi-static stiffness; dynamic stiffness

Citation: Sørum, S.H.; Fonseca, N.; Kent, M.; Faria, R.P. Modelling of Synthetic Fibre Rope Mooring for Floating Offshore Wind Turbines. *J. Mar. Sci. Eng.* **2023**, *11*, 193. https://doi.org/10.3390/jmse11010193

Academic Editor: Luca Martinelli

Received: 16 December 2022
Revised: 6 January 2023
Accepted: 9 January 2023
Published: 12 January 2023

1. Introduction

Synthetic mooring lines offer an alternative to catenary mooring lines in many applications. For deep-water oil and gas, chain mooring becomes too heavy, and the lighter synthetic mooring lines are often used. In the offshore wind industry, floating offshore wind turbines (FOWTs) are being installed at relatively shallow water depths. This often gives catenary mooring lines with little geometric stiffness, which in turn increases the loads in the mooring lines. The lower material stiffness of synthetic mooring lines is then advantageous. In addition, fibre ropes, such as polyester (PET), offer a reduced cost per breaking strength and better fatigue properties than chain. The use of fibre mooring systems may, therefore, contribute to reducing the cost of moorings for FOWTs, aiding future large-scale deployments.

However, modelling of fibre ropes is not straight-forward. The material stiffness is non-linear and dependent on load level, load history, load rate and load path. Loading above the previous highest load level will cause permanent elongation of the rope, mainly due to reorganization of the molecules within the fibres [1]. PET ropes consist of both crystalline and amorphous parts. For slow loading, both parts elongate due to the load and the stiffness is a combination of the stiffness from both. This is typically referred to as the static stiffness, while the quasi-static stiffness which also accounts for creep is more frequently used in analyses. For more rapid loading, only the crystalline parts react to the load. This gives

a higher stiffness, typically referred to as the dynamic stiffness [2]. Both Kwan et al. [2], François and Davies [1], and Falkenberg et al. [3] reports an increase of the dynamic stiffness with the mean tension. François and Davies [1] reports a small dependency of dynamic stiffness on load amplitude for harmonic loading, but not for ropes subjected to wide-band stochastic loads representative of a mooring system. Kwan et al. [1] investigated load amplitudes close to the mean load, and found a larger influence on the dynamic stiffness. They also recommend that the load period (or an equivalent period for stochastic loading) is included in the estimations of dynamic stiffness. François and Davies found this influence to be negligible [1]. Liu et al. [4] found the dynamic stiffness to be dependent on the tension amplitude also for small tension ranges.

Due to the complex stiffness properties, it is not straightforward how fibre ropes should be tested and modelled. Different certification bodies have adapted different test procedures, which may produce very different estimates of both the quasi-static and dynamic stiffness [3]. The approach taken to modelling the properties of fibre ropes also varies between the certification bodies. American Bureau of Shipping (ABS) recommends using a bi-linear stiffness curve, with a quasi-static stiffness below the mean tension, and a dynamic stiffness at higher loads [5]. The recommendation is based on the findings in the Polyester Stiffness Modeling, Testing, and Analysis Joint Industry Project (JIP) [2]. DNV [6] recommends a more elaborate model, based on the Syrope JIP [3,7,8]. This model allows for using the quasi-static stiffness to estimate the mean loads and offsets, while the dynamic stiffness is applied for low-frequency (LF) and wave frequency (WF) motions both above and below the mean tension. Further, the Syrope model considers the permanent elongation caused by loading above the previous maximal load. It is, however, not obvious how this elongation should be handled if tensions above the installation tension can be seen during operation of the turbine. Bureau Veritas recommends a similar approach as the Syrope model [9]. Other models also exist, such as using a lower-bound stiffness for predicting the extreme displacements and an upper-bound stiffness for predicting loads [3,5].

West et al. [10] compares the response predictions of an FOWT when modelling the mooring line stiffness using the linear lower and upper bound material stiffness, as well as a non-linear stiffness model. They found an influence on both the platform motions and accelerations, with differences between the models increasing with the severity of the sea state. A shift in the horizontal platform natural frequency was also observed. Falkenberg et al. [11] compared the Syrope model with the previous recommendations from DNV, using the lower and upper bound material stiffness. An approach with different stiffness values for LF and WF response was also included. The Syrope model was found to predict a shorter fatigue lifetime, while the ultimate limit state (ULS) loads would both increase and decrease depending on the model used for comparison.

This paper aims at comparing the fatigue lifetime and extreme response predictions when using two different formulations for the fibre rope material stiffness, demonstrating how the material model influences the calculated design capacity. This is done using the Syrope model recommended by DNV and the bi-linear stiffness curve recommended by ABS. Further, the paper presents procedures for adaption of sub-rope static and dynamic laboratory test results to fibre rope models and to simulate the material and mooring lines' properties in the context of time domain mooring analysis. The properties of the fibre ropes are determined from tests performed by Bridon-Bekaert, while the SATH FOWT concept from SAITEC is used as the case-study. The FLS and ULS analyses are based on fully coupled time domain simulations.

The paper is organized as follows: A general review on the Syrope and bi-linear models are given in Section 2. The MooringSense project is presented in Section 3. The methods and models are presented in Section 4, including the test procedure for determining the PET rope properties (Section 4.1), and the adaption to the bi-linear and Syrope model (Section 4.1.1). The influence of the model selection on the system properties and predicted FLS and ULS capacity are presented in Section 5, before the results are discussed in Section 6. Finally, the paper is concluded in Section 7.

2. Stiffness Models

This section will provide a general overview of the two stiffness models compared in this study. The rope-specific adaption of the polyester rope properties to the different models are presented in Section 4.1.

2.1. The Syrope Model

The Syrope model [3,7,8] is based on tension-stretch relationships dependent on the load-rate and load-history of the rope, and is illustrated in Figure 1. The original curve (OC) is the tension-strain relationship for a new rope subjected to rapid loading above the previous highest load level. When the rope is loaded slowly, or kept at a constant tension, at tensions above the previous maximum mean tension ($\bar{T}_{max}$), the rope will acquire an additional permanent stretch. This gives the original working curve (OWC). When unloaded or loaded below $\bar{T}_{max}$, the rope stiffness increases and the loading happens along a working curve (WC). Both the OWC and WCs represent the quasi-static stiffness of the rope. A combination of mean tension ($\bar{T}$) and $\bar{T}_{max}$ defines a working point (WP), i.e., the combination of mean tension and strain which dynamic LF and WF response happens around. Consequently, the dynamic properties of the rope is a combination of the dynamic stiffness and a working point, where the working point is dependent both on $\bar{T}_{max}$ (defining the working curve) and $\bar{T}$ (defining the working point).

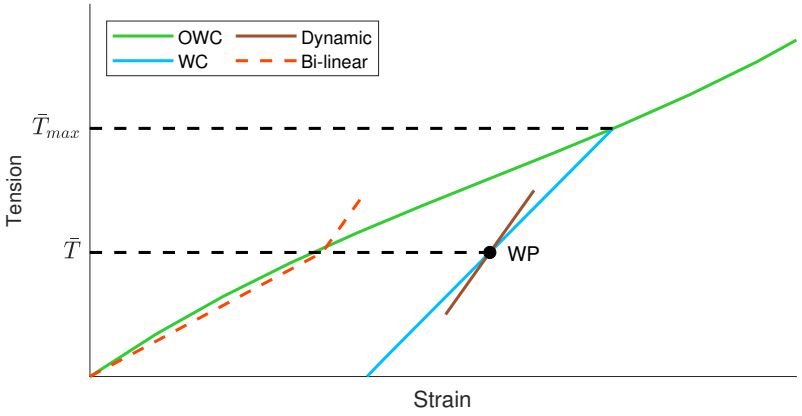

Figure 1. Illustration of the Syrope model (green, blue and brown lines) and bi-linear model (orange line) for a fibre rope under mean tension $\bar{T}$. The historically highest mean tension is given by $\bar{T}_{max}$.

2.2. The Bi-Linear Model

ABS recommends a bi-linear static-dynamic stiffness model [5], as illustrated in Figure 1. The initial section of the stiffness curve represents the quasi-static stiffness, applied up to the mean tension. Above this, the dynamic stiffness is used. The quasi-static stiffness accounts for the load-history by defining three categories of quasi-static stiffness: pre-installation, post-installation and aged rope. These stiffness values should account for both the instantaneous static stiffness and the effect of creep elongation. The standard recommends modelling the dynamic stiffness as dependent on mean tension and load period for FLS, with an additional dependence on load amplitude for ULS.

3. The MooringSense Project

This work is carried out as part of the MooringSense project [12]. The MooringSense project is a collaborative research and innovation project financed under the EU HORIZON 2020 program. The objective is to develop tools and strategies for efficient mooring system integrity management for FOWTs, to reduce operational costs and increase annual energy production. An important component of the MooringSense concept is a digital twin of the mooring system, consisting of information and numerical tools. These tools are based on, or use results from, a fully coupled numerical model of the FOWT. The six tools have the following functionalities:

- Virtual measurements of mooring line loads.
- Continuous calculation of synthetic rope properties.
- Prediction of floater motions.
- Calculation of remaining lifetime.
- Mooring re-analysis
- Calculation of local damages in chains.

The SATH sub-structure concept from SAITEC [13] supporting a 10 MW wind turbine is the reference case for MooringSense. The sub-structure consist of a twin hull platform with cylindrical floaters. Heave plates reduce the wave induced vertical motions. A single point mooring system provides station keeping, while allowing the platform to weathervane with the environmental loads. The mooring system consists of six lines with a bottom chain segment, an intermediate polyester segment and a fairlead chain segment. Figure 2 shows the mooring system layout, while Figure 3 shows the sub-structure. The main properties of the FOWT are given in Table 1, and the mooring line properties are given in Table 2.

Table 1. Main properties of the SATH FOWT.

Parameter	Value
Wind turbine capacity [MW]	10
Length [m]	104.2
Beam (width) [m]	47.5
Hub height [m]	108
Draft [m]	9.4

Table 2. Properties of the mooring system.

	Fairlead Chain	Fibre Rope	Bottom Chain
Length [m]	40	588	150
Diameter [mm]	147	147	147
MBL [tonnes]	2273	885	2273

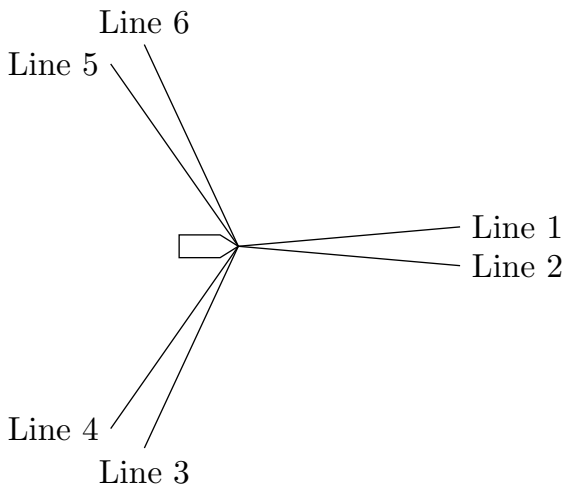

Figure 2. Layout of the mooring system.

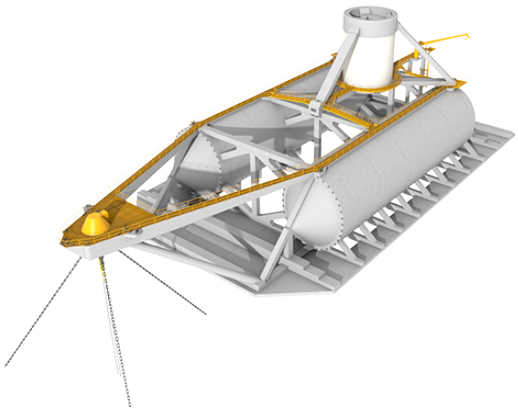

Figure 3. Saitec's SATH substructure [13].

4. Method

The inputs for both the Syrope model and bi-linear model are based on testing of sub-ropes performed by Bridon-Bekaert. Starting with the test procedure, the following sections will also present the adaption of the results to the fibre rope models, the mooring line design, the FOWT and the methods for assessing the mooring line capacity.

4.1. Polyester Sub-Rope Testing and Full Rope Properties

Break-elongation, quasi-static stiffness and dynamic stiffness tests were performed to determine the fibre rope properties. The testing was based on ABS' test procedure [5], but excluding the installation pre-loading test and with reduced load levels for the stiffness test. Figure 4 shows the full testing procedure for determining the stiffness properties, giving the tension history. The strain-tension relationships from the tests are presented in Section 4.1.1. The initial test sequence allows determination of the quasi-static stiffness of the new rope. Following this, ageing of the rope is performed application of high loads and rapid cycling, before tests to determine the quasi-static properties of the aged rope are performed. Finally, the rope was subjected to rapid cycling with varying mean tension and load amplitudes to determine the dynamic stiffness. The secant stiffness when increasing the load level from 1.7% MBL to 12.5% MBL, from 12.5% MBL to 30% MBL, and from 30% MBL to 40% MBL was used to estimate the quasi-static stiffness for the new and aged rope. The dynamic stiffness tests were carried out for mean tensions between 5% MBL and 40% MBL, with tension ranges of 2–30% MBL and periods 12–35 s.

Change in length properties for the full rope were assumed similar to the sub-rope properties, with the full rope capacity being the aggregated capacity of the individual sub-ropes. The full rope is built from a collection of individual sub-ropes, terminated in pairs by splices. The splicing process introduces differences in the sub-rope lengths, leading to non-homogeneous loading of the different sub-ropes. Due to limitations on test bed dimensions (meaning short ropes are tested) and short time under load, testing of a full rope would give a lower tenacity for the full rope than the aggregated tenacity of the sub-ropes. For longer time under load and rope lengths (e.g., more than 50 m) the unbalance in the loading of the ropes is minimized by improvements in the rope and splices bedding-in, as well as fibre creep. The aggregated capacity of the sub-ropes is, therefore, a better representation of the full-rope properties than tests performed on a full rope. For testing the change in length characteristics of fibre ropes, testing of sub-ropes is preferred over full ropes as the obtained results are more accurate and the tests more economical [6].

4.1.1. Adaption to Fibre Rope Models

As the tests were performed in accordance with ABS' procedures, the results can be readily adapted to the bi-linear model. The following assumptions were employed: (1) The static stiffness was taken as either the quasi-static new stiffness, assuming negligible installation tension, or the quasi-static aged stiffness model, assuming the same permanent

elongation as the Syrope model. These will be denoted the bi-linear new and bi-linear aged models, respectively. (2) A constant quasi-static stiffness corresponding to the loading up to 12.5% MBL was assumed appropriate for both ULS and FLS conditions. (3) The dynamic stiffness was assumed a linear fit to the mean tension only:

$$K_d = a + b\bar{T}, \tag{1}$$

where K_d is the dynamic stiffness, $\bar{T}$ is the mean tension, and a and b are coefficients. The dependency of the dynamic stiffness on load period is logarithmic, and therefore typically small [1]. Further, K_d has been seen to vary with tension range when the tension amplitudes are close to the mean tension [2]. Liu et al. [4] recommend including the dependency on tension range for all combinations of mean tension and tension range. For the current rope design, it was assumed that the dynamic stiffness could be modelled as a function of mean tension only, as given by Equation (1). Following the completion of the time-domain simulations, it was verified that the effect of the tension amplitude was small. Including this in the equation for the K_d would change the dynamic stiffness by <3% in the ULS condition, with even smaller differences seen in the FLS analyses.

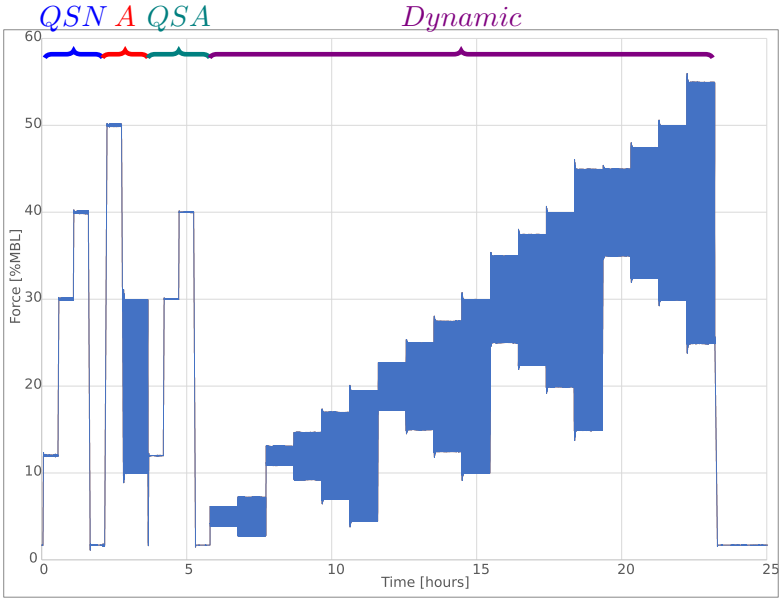

Figure 4. Test procedure for polyester sub-rope. *QSN* = Quasi-static new stiffness test. *A* = ageing of rope. *QSA* = Quasi-static aged stiffness test. *Dynamic* = Dynamic stiffness test.

The following adaptions were made to fit the test data to the Syrope model: (1) The OWC was modelled using the quasi-static new, as the test description for the OWC is similar to the test performed to determined the quasi-static new stiffness [6]. (2) The WCs model the quasi-static stiffness of a rope that has previously been subjected to higher loadings. The quasi-static aged stiffness tests are the closest to this of the performed tests, and the quasi-static aged stiffness curve is used as the working curve. The same curve was employed for all WCs, with a shift along the strain-axis corresponding to the permanent elongation. (3) The dynamic stiffness was assumed a linear fit as function of the mean tension. The OC corresponds to rapid loading to load levels higher than the previous loading. These conditions are not included in the present study, and the OC is not considered.

The resulting fibre rope models are illustrated in Figure 5, for a range of $\bar{T}_{max}$ and $\bar{T}$. The Syrope and bi-linear dynamic stiffness models are equal, while that quasi-static stiffness for the bi-linear model approximately follows the OWC or WC of the Syrope model.

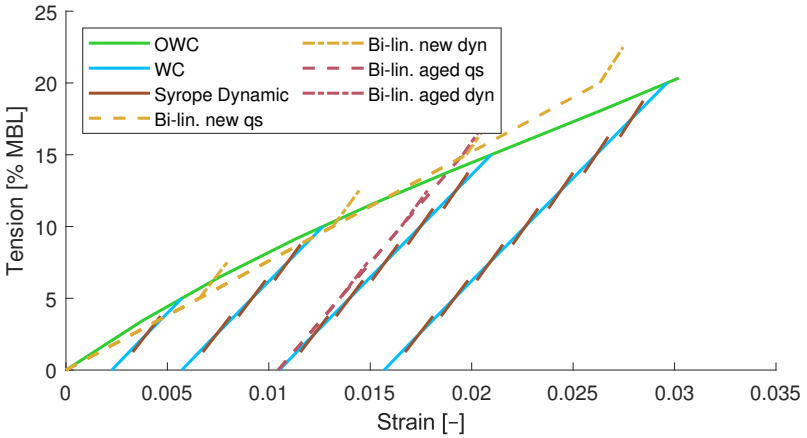

Figure 5. Syrope and bi–linear stiffness models for the fibre rope.

4.2. Simulation of Mooring Line Properties

The mooring lines were modelled in the software RIFLEX v.4.23 [14], which has the Syrope model implemented and is capable of handling non-linear material stiffness curves. The simulations are initiated by adjusting the line lengths to account for the acquired permanent elongation, which is the elongation at zero tension for the WC intersecting the OWC at the historic maximal mean tension, $\bar{T}_{max}$. This is illustrated as ϵ_{perm} in Figure 6. Following this, the static analysis is carried out using the force-elongation relationship defined by the WC to find the mean tension, $\bar{T}$. If $\bar{T} > \bar{T}_{max}$, the current analysis represent a new historic highest mean tension, $\bar{T}_{max}$. $\bar{T}_{max}$ is then iteratively updated until $\bar{T}_{max} = \bar{T}$.

The dynamic stiffness is then calculated in accordance with Equation (1). The mooring lines are elongated so that the dynamic simulations can be performed using the dynamic stiffness, while predicting the quasi-static elongation at $\bar{T}$. This additional elongation is denoted ϵ_{dyn} in Figure 6.

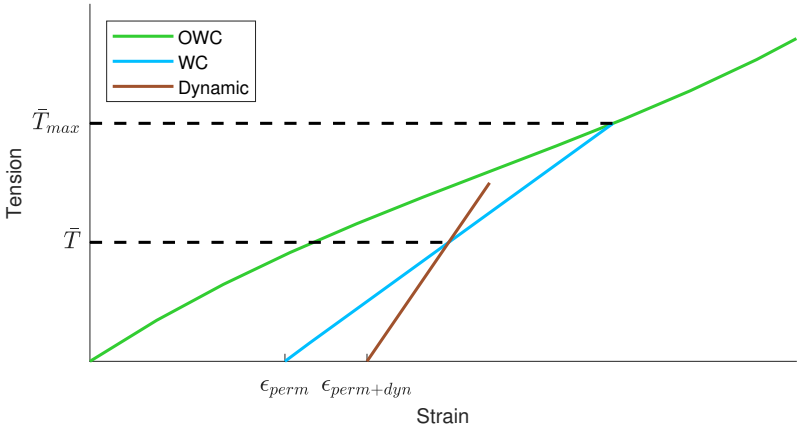

Figure 6. Updating of line lengths and stiffness using the Syrope model. ϵ_{perm} denotes the permanent elongation due to historic loading, ϵ_{dyn} is the additional elongation allowing the dynamic simulations to predict the correct mean elongation. Adapted from DNV RP-E305 [6].

Figure 7 illustrates the simulation process, with the steps in grey being performed as part of the Syrope model implementation in RIFLEX. The steps in white are automated in the simulation workbench SIMA v.4.3.0, which is used for modelling and simulation execution.

When using the bi-linear model, an initial static analysis with the quasi-static material stiffness is performed. This finds the mean tension in all mooring lines, and the material stiffness is updated with the bi-linear stiffness model. Following this, the dynamic analysis is performed. The procedure is illustrated in Figure 7.

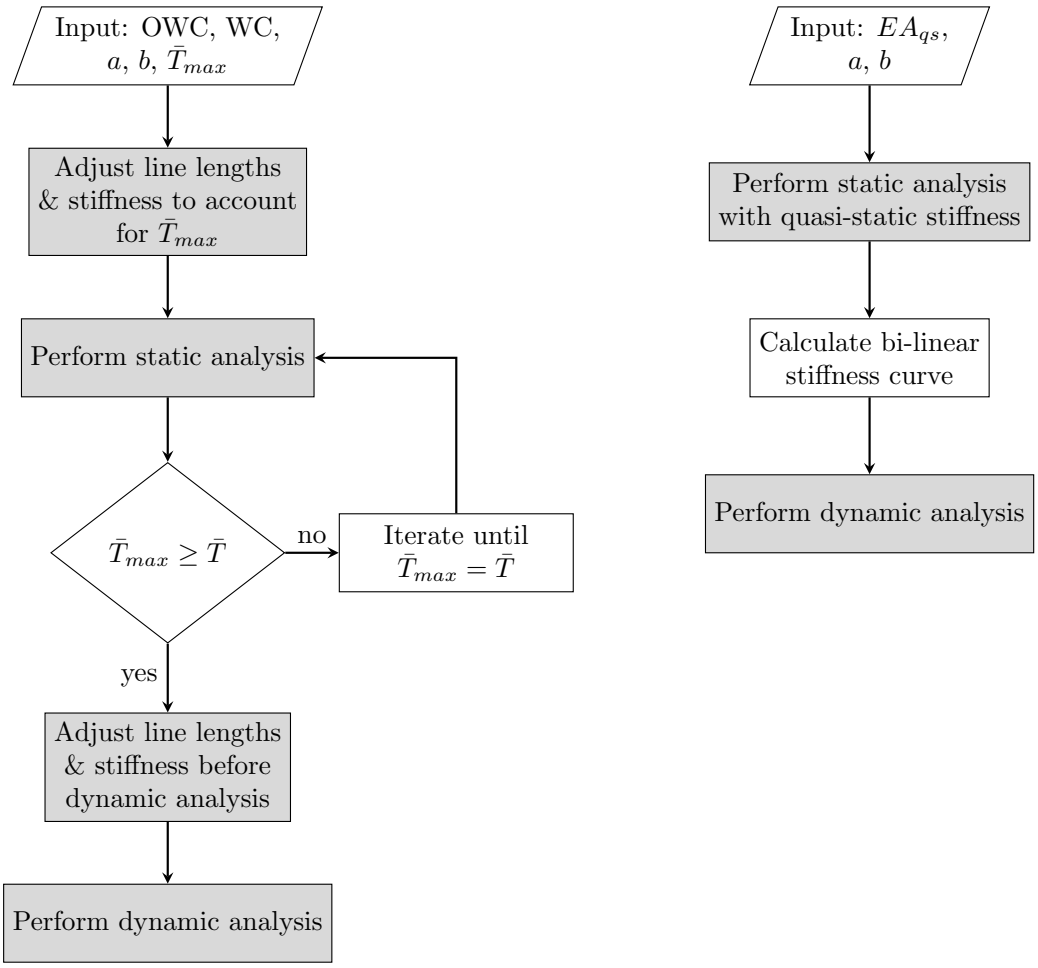

Figure 7. Simulation procedure for updating the mooring line properties for the Syrope model (**left**) and bi-linear model (**right**). The steps in grey are performed in RIFLEX, while the steps in white are performed in SIMA as part of the model and simulation setup.

4.3. Case Study

The effect of using either fibre rope model will be demonstrated using the MooringSense reference case (Section 3) [13,15]. The DTU 10 MW turbine [16] is situated on the platform, and is controlled using the ROSCO open-source controller [17]. The turbine was assumed located at 120 m water depth at Buchan Deep, outside the east coast of Scotland. The environmental conditions were based on the metocean data for the site [18]. ULS capacity is checked using design load case (DLC) 1.6 [19] for rated wind speed, with the wind-speed dependent 50-year significant wave height (H_s, 4.71 m) and mean H_s-dependent wave peak period (T_p, 10.1 s). FLS capacity was checked using DLC 1.2 for 10 wind speeds. H_s for each wind speed was found from a fit of expected H_s vs. wind speed, and T_p was taken as the mean T_p as function of H_s. These are illustrated in Figure 8, together with the probability of occurrence. A surface current velocity of 0.41 m/s was used for all load cases, corresponding to the mean current at the site. To reduce the computational effort, the environmental loads are assumed equally probable to arrive parallel to mooring line groups 1–2, 3–4 and 5–6.

The Syrope model requires $\bar{T}_{max}$ as input. Unless otherwise specified, this is assumed to be the mean tension with a 1-year return period for all mooring lines.

Fatigue damage is calculated in the fairlead chains using the rainflow counting algorithm in WAFO [20]. The S-N curve for studless chain is applied, while mean tension and out-of-plane bending effects are neglected.

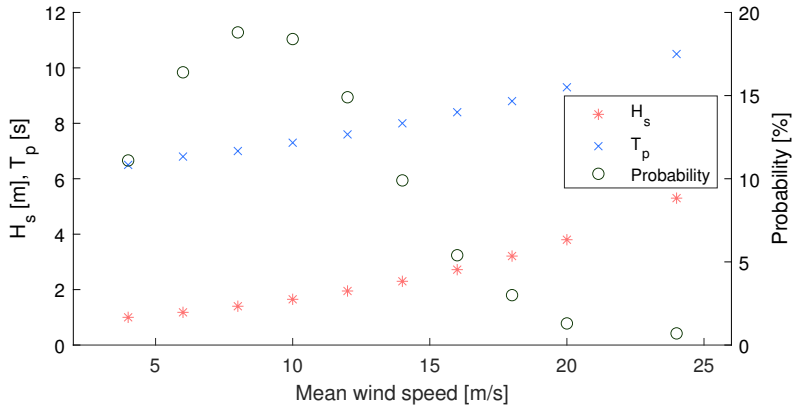

Figure 8. Mean wind speed, H_s, T_p and probability of occurrence for fatigue load cases.

ULS capacity is checked according to DNV ST-0119 [21], with the design tension taken as:

$$T_d = \gamma_{mean} T_{c,mean} + \gamma_{dyn} T_{c,dyn}. \quad (2)$$

Here, γ_{mean} and γ_{dyn} are the safety factors on the mean and dynamic tension. $T_{c,mean}$ and $T_{c,dyn}$ are the characteristic mean and dynamic tension values, i.e., the most probable 1-h extreme response. This is found from 20 seed variations. Assuming consequence class 1, $\gamma_{mean} = 1.3$ and $\gamma_{dyn} = 1.75$.

Simulation Model

The fully coupled simulations are performed with the coupled software SIMO-RIFLEX, with modelling and simulation management performed in the SIMA workbench. The SATH substructure is modelled as a rigid body in SIMO v.4.23 [22], and the flexible mooring lines, wind turbine and tower are modelled in RIFLEX. The hydrodynamic model is based on potential-flow calculations from WAMIT, including linear wave forces, wave drift forces, quadratic current forces and wind forces. Comparisons between model tests and state of the art numerical tools show limitations in estimating viscous and second order effects. Calibration of numerical models towards model tests can significantly improve the accuracy of numerical models. Based on model tests of the SATH [15], viscous loads on the heave plates have been modelled using slender elements. Adjustments were also made for the added mass and global linear damping in heave, pitch and coupled heave-pitch.

Wave and current loads on the mooring system are calculated using Morison's equation, and aerodynamic loads on the tower are modelled as quadratic drag loads. Loads on the rotor are calculated using the blade element momentum theory, with corrections for dynamic wake and stall, tip and hub loss corrections, and yawed inflow correction. The tower and blades are modelled as linear-elastic beam elements, while the mooring lines are modelled as bar elements. Structural damping is modelled as stiffness-proportional Rayleigh damping.

5. Results

The main result of this study is the difference in predicted fatigue utilization when using the two material models. This is presented in Section 5.3, but first the effect on the mooring line and mooring system properties are presented (Section 5.1), and the effect on the natural periods (Section 5.2). Sufficient capacity in ULS is also demonstrated (Section 5.4), where the differences between the models are caused by other mechanisms than in FLS.

5.1. Mooring System Properties

The material models influence the dynamic and quasi-static properties of both the single mooring lines (Figure 9) and the full mooring system (Figure 10). The difference

between the bi-linear stiffness model and the linear dynamic stiffness used in the Syrope model is seen clearly if comparing the single-line dynamic properties for the bi-linear new and Syrope models. For loads above $\bar{T}$, the two models yield similar dynamic stiffnesses, influenced only by differences in the mean tension. Below mean tension, the stiffness is reduced when using the bilinear model. As WF-motions of the platform are inertia-dominated and not influenced by the mooring line stiffness, the displacement at fairlead will be governed by the platform motions. A mooring line modelled with the bi-linear new stiffness curve will experience lower load variations below $\bar{T}$, given similar platform motions. This effect is largest for mooring lines with high tension (large positive displacements in Figure 9), where the geometric stiffness is low and the material stiffness governs. The same is seen for the bi-linear aged model, but here the difference between the quasi-static and dynamic stiffness is much lower. Less differences in the mooring line tensions are then expected if the quasi-static aged model is compared to the Syrope model.

Similar observations can be made for the full mooring system. With taut mooring lines, the dynamic stiffness is close to linear for the Syrope model and the bi-linear aged model. The bi-linear new model yields a non-linear dynamic stiffness, which never follows the static stiffness as the windward and leeward mooring lines experiencing tensions above and below $\bar{T}$ at different times. This results in a mooring system stiffness that is neither completely quasi-static nor dynamic, but rather a mix of these two. The same is seen for the bi-linear aged model, where the dynamic stiffness is lower than for the Syrope model, despite the quasi-static properties being very similar.

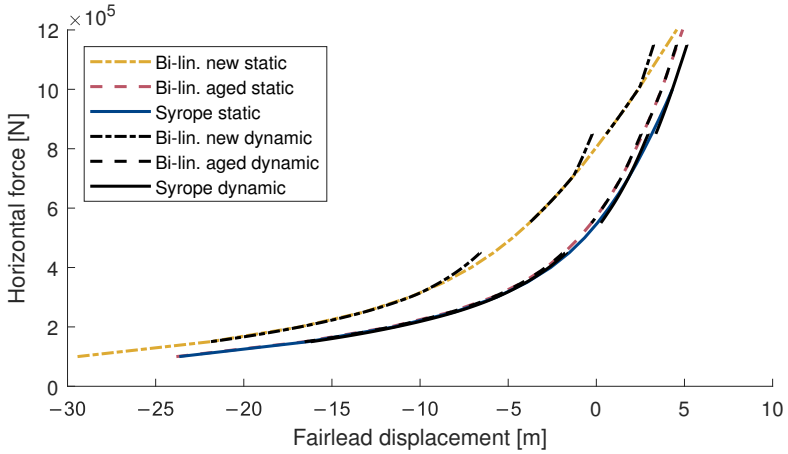

Figure 9. Force–displacementrelationship for a single mooring line using, with dynamic relationships given for loading about mean horizontal forces of 0.3, 0.7 and 1 MN. Fairlead displacement = 0 refers to the installed position of the fairlead.

5.2. Effect on Natural Periods

The differences in the mooring system stiffness influence the natural periods predicted by the two material models. A surge decay test was performed to demonstrate these difference, shown in Figure 11. This shows a clear amplitude-dependence of the natural period predicted when using the bi-linear models, particularly with the bi-linear new model where the difference between the quasi-static and dynamic difference is largest. This is not seen for the Syrope model, and is attributed to the non-linear material stiffness used with the bi-linear model.

5.3. FLS Results

The 1-h fatigue damage at fairlead, scaled by the probability of occurrence, is shown in Figure 12a for the mooring line with the highest 1-hour fatigue damage. For all wind speeds, the Syrope model predicts a higher fatigue damage, with the bi-linear new model predicting the lowest fatigue damage. This also reflects in the predicted fatigue lifetime (Figure 12b), when the environmental directionality is taken into account. The expected

lifetime of the mooring lines using the Syrope model are then reduced by 15 years compared to the bi-linear new model and five years compared to the bi-linear aged model.

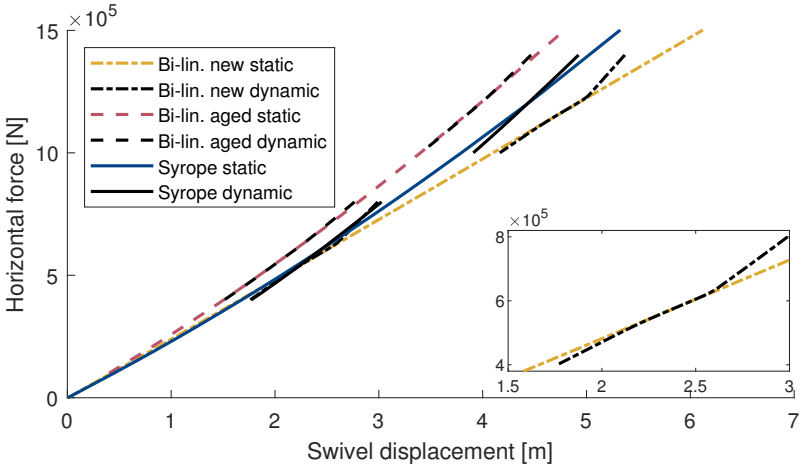

Figure 10. Force–displacement relationship for the full mooring system, with dynamic relationships given for loading about mean horizontal external forces of 0.6 and 1.2 MN. The swivel displacement is given relative to the position of the swivel when there are no external loads on the system.

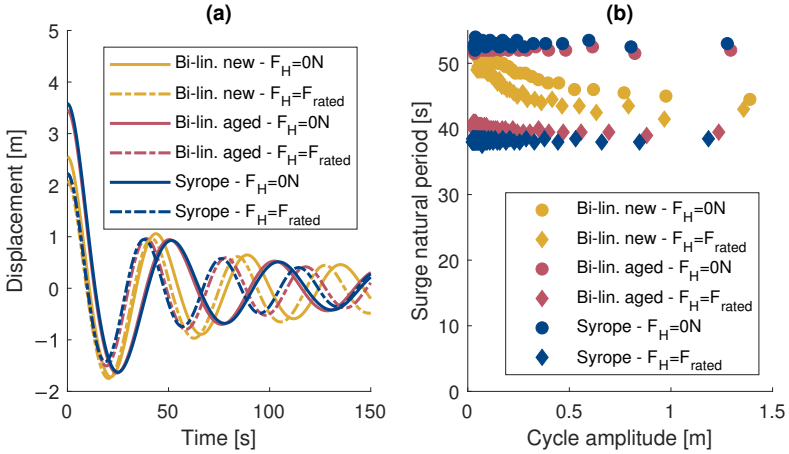

Figure 11. (**a**) Time series of the surge decay test. (**b**) Estimated natural period as function of surge amplitude.

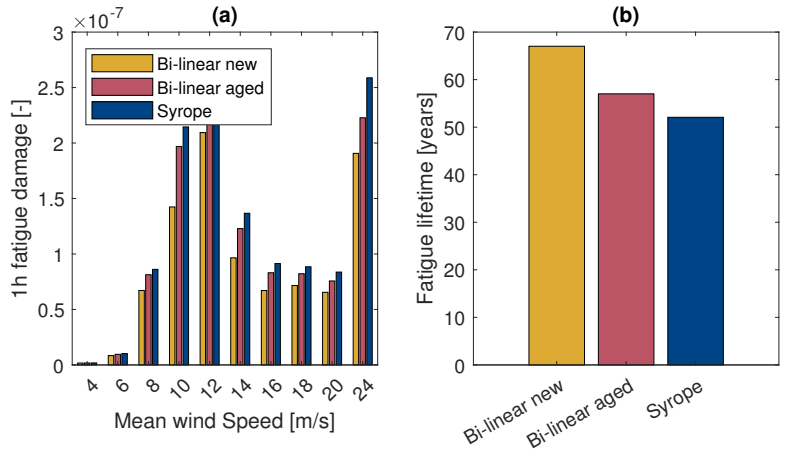

Figure 12. (**a**) 1-h fatigue damage in the upwind fairlead chain, multiplied by probability of occurrence. (**b**) Fatigue lifetime in the fairlead chain if the environmental loads are equally probably to arrive parallel to the three mooring line groups.

The differences between the models are primarily caused by the reduced stiffness in the quasi-static region of the bi-linear model. This is illustrated in Figure 13, showing the dynamic tension in mooring line 1 for wind speed 24 m/s. For tensions above $\bar{T}$, the models yield similar tension estimates. Below the mean tension, the load amplitudes are significantly reduced when using the bi-linear new model, and somewhat reduced when using the bi-linear aged model. This is caused by the lower stiffness in the bi-linear model, which gives lower tension variations below $\bar{T}$. This is illustrated in Figure 14a, where each point corresponds to the tension-elongation observed for wind speed 12 m/s.

The effect on the tension distribution is shown in Figure 14b for wind speed 12 m/s, where the bi-linear model shifts the probability of the instantaneous tension towards $\bar{T}$ for $T < \bar{T}$. This leads to reduced tension amplitudes, which in turn gives reduced fatigue damage estimates compared to the Syrope model.

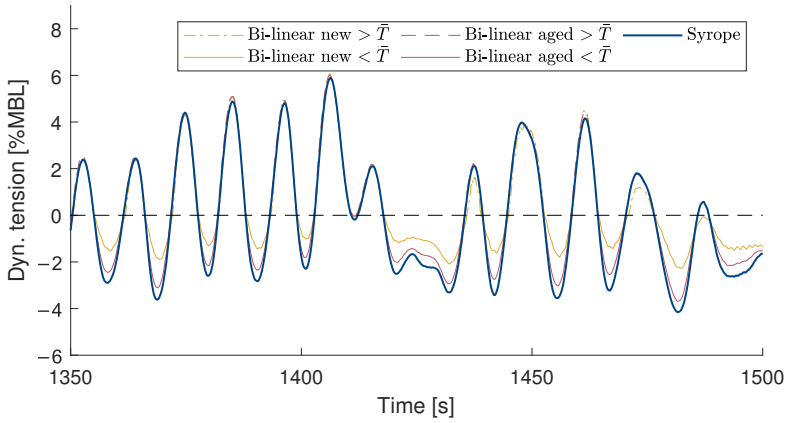

Figure 13. Sample dynamic tension time series for mooring line 1 under wind speed 24 m/s. The bi-linear and Syrope models show good agreement for tensions above $\bar{T}$, while the tension amplitudes are reduced for the bi-linear model below $\bar{T}$.

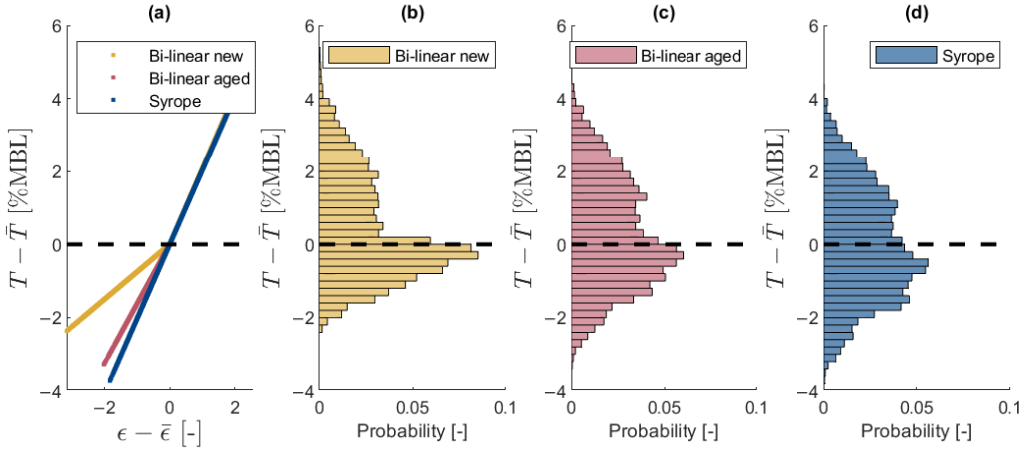

Figure 14. (**a**) Tension-elongation relationship calculated from the time series of tension in mooring line 1 under wind speed 12 m/s. $\bar{T}$ and the corresponding mean elongation, $\bar{\epsilon}$ has been removed, yielding the dynamic variations in the mooring line. (**b**–**d**) Empirical probability distribution of the instantaneous dynamic tension in mooring line 1 for wind speed 12 m/s.

5.4. ULS Results

The ULS design tension (T_d) for the load case considered is shown in Figure 15a for the Syrope and bi-linear new model. The utilization of both the fairlead chain and fibre rope is well below the allowable 95% MBL [21]. This has been considered acceptable, given that a full ULS design is not carried out. The figures also shows that the design tension in the windward lines is consistently 10% higher when using the bi-linear new model. Figure 15b breaks down the design tension of the fibre in mooring line 1 into the different components.

The majority of the difference comes from the pretension, which is lower for the Syrope and bi-linear aged models due to the permanent elongation. For the bi-linear aged and Syrope model, the extreme tensions are close to identical.

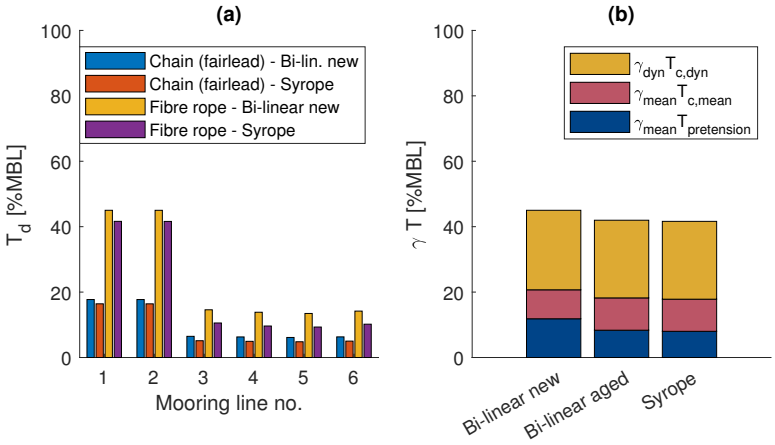

Figure 15. (**a**) ULS design tension in the fairlead chain and fibre rope when applying the bi-linear and Syrope models. (**b**) Contribution to the design tension from pretension, mean environmental loads and dynamic loads.

6. Discussion

The differences between the Syrope and bi-linear model are caused by the updated permanent elongation in the Syrope model and the use of quasi-static stiffness in the bi-linear model during half-cycles corresponding to $T < \bar{T}$. Use of the quasi-static stiffness primarily influences the fatigue lifetime predictions, yielding longer lifetimes for the bi-linear model. The difference between the Syrope and bi-linear model is dependent on the difference between the quasi-static and dynamic stiffness. In the current study, the dynamic stiffness is 2.6–2.8 times the quasi static stiffness for the bi-linear new model, while the ratio is between 1.18 and 1.26 for the bi-linear aged model. Ratios of 1.5–3 is reported for polyester ropes in the literature [1,2,23], while ratios as high as 4 have been reported for other fibre ropes as nylon [24]. The suitability of the bi-linear model for fatigue analysis seems to depend on the properties of the fibre rope being analysed, as too large differences between the quasi-static and dynamic stiffness will artificially reduce the range of the tension cycles and predict an increased lifetime.

For extreme loads, the difference between the bi-linear and Syrope model depends mainly on the permanent elongation of the mooring lines. As there is no established practice for how to install fibre rope mooring lines for FOWTs, the permanent elongation at installation is not given. If the mooring lines are pre-stretched to a load level similar to the ULS utilization, the permanent elongation is taken out and the bi-linear and Syrope models yield similar extreme loads. If no, or limited, pre-tensioning is performed, permanent elongation will occur during the operation of the turbine. This will be captured by the Syrope model, provided an adequate load history is applied. This in turn yields more accurate ULS results, and may also influence the FLS results for cases where the properties of the mooring system are sensitive to changes in the mooring line lengths.

However, it is not clear how this load history-dependency should be taken into account in the design. Unequal loading of the mooring lines will yield different mooring line properties, and two realizations of the same long-term environment may yield different ULS and FLS loads in the mooring system depending on the timing and sequence of storms. No specific guidance is provided in DNV's standards, besides stating that "If the mean tension in any of the lines is higher than the preceding highest working tension then the working curve for these lines needs to be updated" [6].

Conventional structural health monitoring systems adapted from the oil and gas industry are not applicable for floating offshore wind farms, due to the large number of

mooring lines, low reliability and high cost. The MooringSense concept is based on a high-fidelity model of the FOWT, using motion measurements to predict the mooring line forces [12]. Accurate modelling of the mooring line properties and accurate estimation of the accumulated fatigue damage is crucial for the success of such a concept. The Syrope model offers both of these properties, allowing for updating both ULS loads and lifetime fatigue damage.

7. Conclusions

This paper investigates the effect of modelling polyester mooring lines using the bi-linear stiffness model recommended by ABS and the Syrope stiffness model recommended by DNV.

When applied to the taut mooring system of a floating offshore wind turbine, the bi-linear stiffness curve was found to artificially reduce the fatigue damage in the fairlead chain for cases where there is a significant difference between the quasi-static and dynamic stiffness of the fibre ropes. This was caused by the application of the quasi-static polyester stiffness for load levels below the mean tension, giving a reduction in the tension amplitudes. If the difference between the quasi-static and dynamic stiffness is small, this effect reduces and the bi-linear and Syrope models yield more similar lifetime estimates. Designers are, therefore, recommended to consider the quasi-static and dynamic properties of the fibre rope when choosing material model for design analyses.

The two models predict similar environmental contributions to the extreme tensions. Only the pretension varies, if the permanent elongation and/or quasi-static stiffness predicted is different in the two models. This can be taken into account by considering the load history for the Syrope model. Using the bi-linear model, these values must be determined by the designer. Further, the bi-linear model introduces an artificial amplitude-dependency in the horizontal motion natural period in cases where the difference between the quasi-static and dynamic stiffness is significant.

Author Contributions: Conceptualization, S.H.S. and N.F.; Methodology, S.H.S., M.K. and R.P.F.; Software, S.H.S.; Validation, S.H.S. and N.F.; Formal analysis, S.H.S., M.K. and R.P.F.; Investigation, S.H.S.; Resources, N.F.; Data curation, S.H.S., N.F., M.K. and R.P.F.; Fibre rope lab testing and post-processing of data, M.K. and R.P.F.; Writing—original draft preparation, S.H.S.; Writing—review and editing, S.H.S., N.F., M.K. and R.P.F.; Visualization, S.H.S.; Supervision, N.F.; project administration, N.F.; Funding acquisition, N.F. All authors have read and agreed to the published version of the manuscript.

Funding: This research was funded by the European Union's Horizon 2020 research and innovation programme under grant agreement No. 851703 (project MOORINGSENSE).

Institutional Review Board Statement: Not applicable.

Informed Consent Statement: Not applicable.

Data Availability Statement: Not applicable.

Conflicts of Interest: The authors declare no conflict of interest. The funders had no role in the design of the study; in the collection, analyses, or interpretation of data; in the writing of the manuscript; or in the decision to publish the results.

Abbreviations

The following abbreviations are used in this manuscript:

FOWT	Floating offshore wind turbine
PET	Polyester
ABS	American Bureau of Shipping
JIP	Joint industry project
LF	Low frequency
WF	Wave frequency
ULS	Ultimate limit state

OC	Original curve
OWC	Original working curve
WC	Working curve
WP	Working point
MBL	Minimum breaking load

References

1. François, M.; Davies, P. Characterization of Polyester Mooring Lines. In Proceedings of the ASME 2008 27th International Conference on Offshore Mechanics and Arctic Engineering, Estoril, Portugal, 15–20 June 2008; American Society of Mechanical Engineers: New York, NY, USA, 2008; Volume 1, pp. 169–177.
2. Kwan, C.T.; Devlin, P.; Tan, P.L.; Huang, K. Stiffness Modeling, Testing, and Global Analysis for Polyester Mooring. In Proceedings of the ASME 2012 31st International Conference on Offshore Mechanics and Arctic Engineering, Rio de Janeiro, Brazil, 1–6 July 2012; American Society of Mechanical Engineers: New York, NY, USA, 2012; Volume 1, pp. 777–785.
3. Falkenberg, E.; Yang, L.; Åhjem, V. The Syrope Method for Stiffness Testing of Polyester Ropes. In Proceedings of the ASME 2018 37th International Conference on Ocean, Offshore and Arctic Engineering, Madrid, Spain, 17–22 June 2018; American Society of Mechanical Engineers: New York, NY, USA, 2018; Volume 1, p. V001T01A067.
4. Liu, H.; Huang, W.; Lian, Y.; Li, L. An experimental investigation on nonlinear behaviors of synthetic fiber ropes for deepwater moorings under cyclic loading. *Appl. Ocean Res.* **2014**, *45*, 22–32. [CrossRef]
5. ABS. *The Application of Fiber Rope for Offshore Mooring*; ABS: Spring, TX, USA, 2021.
6. *DNV-RP-E305*; DNV-RP-E305 Design, Testing and Analysis of Offshore Fibre Ropes. DNV: Høvik, Norway, 2021.
7. Falkenberg, E.; Åhjem, V.; Yang, L. Best Practice for Analysis of Polyester Rope Mooring Systems. In Proceedings of the Offshore Technology Conference, Houston, TX, USA, 1–4 May 2017.
8. Falkenberg, E.; Yang, L.; Åhjem, V. Spring-Dashpot Simulations of Polyester Ropes: Validation of the Syrope Model. In Proceedings of the ASME 2019 38th International Conference on Ocean, Offshore and Arctic Engineering, Glasgow, UK, 9–14 June 2019; ASME: New York, NY, USA, 2019; p. V001T01A050.
9. *NR493*; Classification of Mooring Systems for Permanent and Mobile Offshore Units. Bureau Veritas: Paris, France, 2021.
10. West, W.M.; Goupee, A.J.; Viselli, A.M.; Dagher, H.J. The Influence of Synthetic Mooring Line Stiffness Model Type on Global Floating Offshore Wind Turbine Performance. *J. Phys. Conf. Ser.* **2020**, *1452*, 012044. [CrossRef]
11. Falkenberg, E.; Åhjem, V.; Larsen, K.; Lie, H.; Kaasen, K.E. Global Performance of Synthetic Rope Mooring Systems: Frequency Domain Analysis. In Proceedings of the ASME 2011 30th International Conference on Ocean, Offshore and Arctic Engineering, Rotterdam, The Netherlands, 19–24 June 2011; American Society of Mechanical Engineers: New York, NY, USA, 2011; Volume 1, pp. 507–514.
12. Puras Trueba, A.; Fernández, J.; Garrido-Mendoza, C.A.; La Grotta, A.; Basurko, J.; Fonseca, N.; Arrabi, I.; Savenije, F.; Pourmand, P. A Concept for Floating Offshore Wind Mooring System Integrity Management Based on Monitoring, Digital Twin and Control Technologies. In Proceedings of the ASME 2021 40th International Conference on Ocean, Offshore and Arctic Engineering, Virtual, 21–30 June 2021; American Society of Mechanical Engineers: New York, NY, USA, 2021; Volume 9, p. V009T09A019.
13. Saitec Offshore Technologies. SATH Technology. Available online: https://saitec-offshore.com/sath/ (accessed on 24 August 2022).
14. SINTEF Ocean . *Riflex 4.23.0 Theory Manual*; SINTEF Ocean: Trondheim, Norway, 2022.
15. Fonseca, N.; Nybø, S.; Rodrigues, J.; Gallego, A.; Garrido, C. Identification of wave drift forces on a floating wind turbine sub-structure with heave plates and comparisons with predictions. In Proceedings of the ASME 2022 41st International Conference on Ocean, Offshore and Arctic Engineering, Hamburg, Germany, 5–10 June 2022; ASME: New York, NY, USA, 2022; p. OMAE2022-81467.
16. Bak, C.; Zahle, F.; Bitsche, R.; Kim, T.; Yde, A.; Henriksen, L.C.; Natarajan, A.; Hansen, M.H. *Description of the DTU 10 MW Reference Wind Turbine*; Technical Report; DTU Wind Energy: Roskilde, Denmark, 2013.
17. NREL. *ROSCO*; Version 2.4.1; NREL: Golden, CO, USA, 2021.
18. Statoil. *Hywind Buchan Deep Metocean Design Basis RE2014-002*; Technical Report; Statoil: Stavanger, Norway, 2014.
19. *DNVGL-ST-0437*; DNVGL-ST-0437 Loads and Site Conditions for Wind Turbines. DNVGL: Høvik, Norway, 2016.
20. WAFO-Group. *WAFO—A Matlab Toolbox for Analysis of Random Waves and Loads—A Tutorial*; Centre for Mathematical Sciences, Lund University: Lund, Sweden, 2017.
21. *DNVGL-ST-0119*; Floating Wind Turbine Structures. DNVGL: Høvik, Norway, 2018.
22. SINTEF Ocean. *SIMO 4.23.0 Theory Manual*; SINTEF Ocean: Trondheim, Norway, 2022.

23. Depalo, F.; Wang, S.; Xu, S.; Guedes Soares, C.; Yang, S.H.; Ringsberg, J.W. Effects of dynamic axial stiffness of elastic moorings for a wave energy converter. *Ocean Eng.* **2022**, *251*, 111132. [CrossRef]
24. Varney, A.S.; Taylor, R.; Seelig, W. Evaluation of wire-lay nylon mooring lines in a wave energy device field trial. In Proceedings of the 2013 OCEANS MTS/IEEE, San Diego, CA, USA, 23–27 September 2013; pp. 1–5.